Composites: Part A 40 (2009) 1082–1089

Contents lists available at ScienceDirect

Composites: Part A

journal homepage: www.elsevier.com/locate/compositesa

# Basalt fiber–epoxy laminates with functionalized multi-walled carbon nanotubes

Wei Chen [a,*], Hongbin Shen [b], Maria L. Auad [c], Changzheng Huang [a], Steven Nutt [a]

[a] M.C. Gill Composites Center, Materials Science Department, Vivian Hall of Engineering 406, University of Southern California, Los Angeles, CA 90089-0241, USA
[b] Research & Development, M.C. Gill Corporation, 4056 Easy Street, El Monte, CA 91731-1087, USA
[c] Polymers and Fiber Engineering, 103 Textile Building, Auburn University, AL 36849-5327, USA

ARTICLE INFO

*Article history:*
Received 20 November 2008
Received in revised form 22 April 2009
Accepted 22 April 2009

*Keywords:*
A. Carbon nanotubes
A. Nano composites
A. Laminate
B. Mechanical properties
C. Elastic properties

ABSTRACT

Cross-ply laminates reinforced with basalt fibers and functionalized multi-walled carbon nanotubes (MWCNTs) were fabricated from unidirectional epoxy prepregs. MWCNTs with varied surface conditions were prepared by oxidization or esterification, and then dispersed into a DGEBA epoxy system. The dispersion of the MWCNTs in the epoxy was improved by surface modification, resulting in improved composite mechanical properties as well. Significant increases in elastic modulus and strength were observed for epoxies with functionalized MWCNTs, especially for esterified species. When MWCNT – filled epoxies were used as matrices for basalt fiber/epoxy laminates, however, the reinforcement effects of MWCNTs on the composite elastic modulus exceeded micromechanics based semi-empirical predictions and were independent of surface functionalization. SEM morphological observations and the results of the micromechanical model revealed that nanotube re-distribution and orientation during processing was responsible for the enhancement of fiber-dominated mechanical properties. This work demonstrated the feasibility of in situ alignment and dispersion of functionalized nanotubes in multi-scale composite laminates.



## 1. Introduction

Several approaches can be employed to improve the properties of fiber-reinforced epoxies. One approach is to select fiber reinforcements which optimize specific thermal, mechanical, chemical, electrical, or optical properties [1–3]. A second approach is to toughen the matrix and overcome the inherent brittleness of epoxy systems through techniques such as rubber/thermoplastic toughening or epoxy composition modulation [4,5]. A third alternative is to optimize the fiber–matrix interface to enhance the stress transfer properties [6,7]. More recently, multi-scale approaches have been explored to design optimized microstructures at multiple reinforcement length scales [8–11]. These approaches typically attempt to incorporate both nano-scale and micro-scale reinforcements.

Fiber-reinforced epoxy composites filled with nano-particles afford the opportunity to improve the bulk composite properties with minimal sacrifice of other properties of the composites. Among nano reinforcements, multi-walled carbon nanotubes (MWCNTs) stand out because of the ultra-high strength/stiffness [12], large aspect ratio, and relative affordability. Examples of multi-scale composites utilizing MWCNT-filled epoxies in conventional fiber-reinforced composites (FRCs) have been reported. For example, Thostenson et al. [13,14] demonstrated that the anchorage of MWCNTs onto carbon fibers through either direct CVD growth or electrophoresis selectively tailored the "interface properties". In other work, Qiu et al. [15] and Gojny et al. [16] reported that MWCNTs enhanced the electrical properties and the interlaminar shear strength respectively, while preserving or enhancing tensile properties, thus improving "matrix properties".

Despite the temptation to assemble or organize ordered nanotube arrays into composites [17,18], direct dispersion of MWCNTs with tailored surface properties, offers the most practical route because of the simplicity and compatibility with existing composite processing methods. Three key processing challenges are associated with direct CNT incorporation – nanotube dispersion, interfacial bonding, and alignment [19,20]. The dispersion and interfacial bonding issues can be addressed by identifying a suitable nanotube surface modification, which not only disperses the MWCNTs in the resin system but also facilitates stress transfer at the interface through the formation of covalent bonds [21,22]. In addition, high shear force, electric field, and magnetic field have been used successfully to align CNTs in polymer matrices [23–25]. However, these studies have not addressed the influence of processing conditions and CNT surface modification on CNT dispersion and alignment, although this is understandable, given the complexity of composite systems with multiple reinforcement length scales and processing stages.

* Corresponding author. Tel.: +1 213 740 4339; fax: +1 213 740 7797.
*E-mail address:* weichen@usc.edu (W. Chen).

1359-835X/$ - see front matter © 2009 Elsevier Ltd. All rights reserved.
doi:10.1016/j.compositesa.2009.04.027

In the present study, multi-walled carbon nanotubes were grafted with epoxy-compatible surface modifiers [26] before being dispersed directly into the epoxide. The resultant nanotube-filled epoxies were used as matrices in composite laminates reinforced with continuous basalt fibers, selected for the unique thermal, mechanical, and chemical characteristics. The morphology and mechanical behaviors of the nanotube reinforced epoxies (NEs) were analyzed and related to those of NE/basalt laminates in order to elucidate the composition, processing, structure, and property relationship in these hierarchically reinforced composites.

## 2. Experiment

### 2.1. Materials

Raw MWNTs (raw-CNTs) were obtained from a commercial source (Nanotech Port Co. Ltd., Shenzhen., China). The nanotubes were produced by chemical vapor deposition (CVD), and contained ~5 wt% impurities, consisting primarily of amorphous carbon and transition metals. The nanotubes were 5–15 μm in length and 20–60 nm in diameter. A di-glycidyl ether of bisphenol A (DGEBA) type epoxy resin (EPON 828, Miller–Stephenson Chemical Co. Inc.) was selected as the matrix material. The epoxy was used in combination with a curing agent and an accelerator (DICY and Omicure, respectively, Air Products & Chemicals, Inc.) to prepare the composites.

$H_2SO_4$, HCl, and $HNO_3$ were generic chemicals (VWR Scientific) used during the oxidation. Triphenylphosphine (TPP, from Aldrich) was employed as a catalyst to facilitate the esterification reaction that attached phenyl glycidyl ether (PGE, Aldrich) onto the acidified carbon nanotubes. Cellulose acetate and PTFE membranes (VWR and Fisher Scientific) were used during the filtration of MWCNTs. DMF, THF, and anhydrous ethanol were used as solvents (VWR Scientific).

Basalt fiber is made by extrusion (fiber spinning) of molten basalt. Basalt is composed of the minerals plagioclase, pyroxene, and olivine, and exhibits good and chemical resistance. The fiber also exhibits high strength and modulus, and is thus competitive with glass fibers as a composite reinforcement. The basalt fibers used in this study (Rov 68-680/10/Int/Ext., BASALTEX, a division of MASUREEL Holding nv, Belgium) exhibited the following properties: a melting point = 1350 °C ± 100, diameter = 10 μm ± 1.5, tensile modulus = 84 GPa ± 3, and the sizing type was silane.

### 2.2. Chemical modification of MWCNTs

MWCNTs (5 g) were dispersed in 500 ml of concentrated 3:1 $H_2SO_4$/70% $HNO_3$ following the procedure used by Liu et al. [27] Moderate oxidation while maintaining a high MWCNT aspect ratio was achieved by 30 min sonication and 30 min stirring at room temperature. After the acid treatment and exhaustive washes with deionized water, HCl was added to the acid mixture to facilitate the termination of CNT surface defects with carboxylic acid groups, rather than carboxylate. The solution was again extensively washed with deionized water until the pH value of the decantate became the same as deionized water. The acid-treated MWCNTs (denoted as o-CNTs) were collected on a 0.45 μm cellulose acetate membrane by vacuum filtration and were dried in a vacuum oven at 80 °C for 24 h.

Some of the o-CNTs were esterified through a procedure similar to the one reported by Chen et al. [26]. The esterification was carried out by mixing milled o-CNTs and PGE in a DMF solution with TPP as the catalyst. The mixtures were refluxed in an oil bath heated to 150 °C under inert gas ($N_2$) atmosphere for 36 h. These esterified nanotubes with phenyl and *beta*-hydroxyl functionalities on the surface were denoted as the PGE-CNTs. After the treatment, the nanotubes were thoroughly washed with anhydrous ethanol, collected with the PTFE membrane, and dried in a vacuum oven at 80 °C for 24 h.

### 2.3. Composite preparation

#### 2.3.1. Nano-epoxy coupons (NE coupons)

The raw-CNTs, o-CNTs, and PGE-CNTs were milled and dispersed in THF using a bath sonication for 10 min. The epoxy was mixed with THF (1:1 by volume) in a dual-axis high-speed shear mixer (Keyence HY501). The two mixtures were blended for another 10 min and degassed for 5 min in the mixer. The resultant suspension was denoted as nanotube-filled epoxy (NE). Afterwards, THF was evaporated at 80 °C in a vacuum chamber for 48 h. Finally, the curing agent and the accelerator were added to the NE at 4.21 phr and 1.05 phr, respectively. The epoxy system was then mixed and degassed again in the mixer prior to casting. The off-stoichiometry epoxy composition was optimized for filament winding/hot press processes and was used throughout this work. The blend was cast into an aluminum mold pretreated with epoxy mold release to produce the NE specimens. The curing cycle was 1 h at 120 °C and post curing at 160 °C for 3 h. NE specimens were prepared at 0.25, 0.5, and 1.5 vol% MWCNT loadings (see Ref. [28] for the estimation of vol%. The percentage of CNTs refers to the fraction of CNT in epoxy resin throughout this work unless otherwise stated). Five dogbone-shaped NE coupons (63.5 mm × 9.53 mm × 3.2 mm, ASTM D638, type V) were cut and polished from each specimen for tensile test. Residual samples were milled into powder for Differential Scanning Calorimetry (DSC) tests. Following the procedure described above, control samples from pure epoxy resin were also prepared and tested for comparison.

#### 2.3.2. Multi-scale reinforced laminates (MSRs)

The NEs were also used to fabricate the MSR specimens. Unidirectional prepreg was made on a lab-scale drum-winding machine, where basalt fibers were pulled through a resin bath before being wound onto a spinning drum at preset rates. The resin bath contained NE (0 vol%, 0.5 vol% or 1.5 vol% MWCNT loading), the curative and the initiator, which were prepared beforehand using the same mixing and degas procedure mentioned above except that THF was used as diluent at this stage. The unidirectional prepreg was cut from the drum and heated at 60 °C for 20 min. Four plies of prepreg were cut and stacked in a (0/90/90/0) sequence. Lamination was performed using a hot press at 120 °C and 100 psi (~0.69 MPa) pressure for 1 h, followed by a post-cure at 160 °C for 3 h. Finally, laminated MSR samples were cut into five tensile coupons (2.54 cm × 20.32 cm × 0.05 cm) with 3.81 cm tabs glued to both ends of each coupon.

### 2.4. Characterization

The o-CNTs and PGE-CNTs were observed by transmission electron microscopy (TEM, Philips EM420, 120 KV). The weight loss, or defunctionalization of modified MWCNTs, was recorded by thermogravimetric analyses (TGA) at a temperature ramp of 10 °C per minute to a maximum of 800 °C under constant nitrogen flow. The attachment of functional groups on the surface of MWCNTs was verified by FTIR spectroscopy in transmission mode (Nicolet 4700). TGA and FTIR data were reported in Ref. [26].

DSC tests were performed (DSC2920, TA Instruments) using milled NE powder. The samples were heated from 25 °C to 250 °C at 10 °C/min ramp rate with a temperature modulation of ±1 °C/min. The glass transition temperatures were obtained at mid-point of the transition step. The microscopic morphology of the NE and

MR composites was both investigated by SEM (Cambridge 360 at 20 kV). Brittle fracture surfaces (pre-chilled by liquid nitrogen) were sputter-coated with gold prior to observation. Tensile tests were performed on NE coupons and MSR composites using a universal testing machine according to ASTM D638 (specimen type V, crosshead speed: 0.5 mm/min; gauge length: 7.5 mm) and ASTM D3039 (crosshead speed: 0.5 mm/min; gauge length: 127 mm) respectively.

## 3. Results and discussion

### 3.1. Functionalized MWCNTs

As described above, MWCNTs were functionalized through either an oxidation or an esterification scheme, details of which have been reported elsewhere [26]. The functionalized nanotubes (o-CNT and PGE-CNT) are shown in TEM images in Fig. 1. Inspection of the entire sample area revealed that structural integrity of the graphite layers was preserved and CNT aspect ratios of over 100 were maintained. The observed nanotube diameters range from ~20 to 60 nm, which confirmed the information from the supplier. Through the introduction of epoxy-compatible surface functionalities (such as carboxyls and hydroxyls [29]), solubility and reactivity compatibilization was attained between the MWCNTs and the matrix precursor [21]. CNT surface modification improved nano-particle dispersion and facilitated the interface stress transfer through the formation of covalent bonds, leading to the morphological and mechanical properties discussed next.

### 3.2. Nanotube reinforced epoxies (NEs)

SEM inspection of the NE composite fracture surface revealed that chemical functionalization improved nanotube dispersion and appeared to enhance interfacial bonding (Fig. 2). The epoxy containing raw-CNTs showed CNT agglomerations at the length scale of micrometers adjacent to extended CNT-devoid regions (Fig. 2b). Debonded raw-CNTs were also apparent, as shown in the inset of Fig. 2b (suggest you add outline or frame to inset to highlight). In contrast, the inclusion of functionalized nanotubes altered the fracture surface features of neat epoxy dramatically. Prominent parabolic features and "ductile" bands surrounding MWCNTs (indicated by arrows in Fig. 2c and d) were observed in the o-CNT and PGE-CNT systems respectively, in contrast to the fast fracture surface of the neat epoxy. These fracture surface

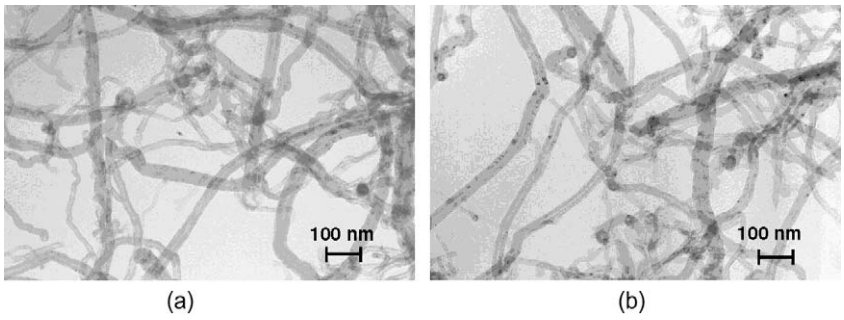


**Fig. 1.** TEM image of o-CNTs (a) and PGE-CNTs (b).

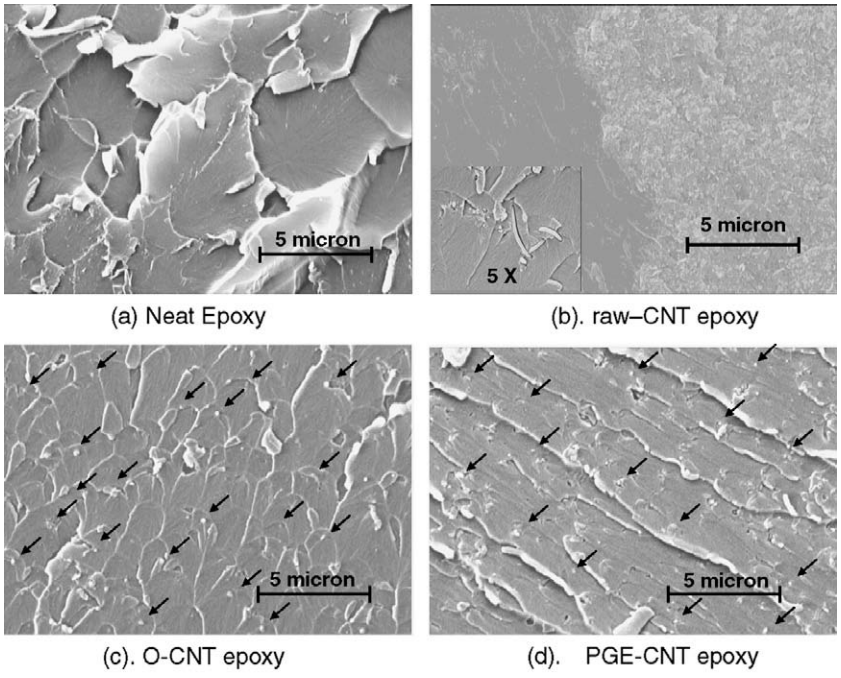


**Fig. 2.** SEM images of fracture surface of NEs. All specimens have a CNT loading of 0.5 vol%.

**Table 1**
Glass transition temperatures (DSC) for NEs at different CNT loadings.

| | 0 vol% | $T_g$ (°C), 0.25 vol% MWCNTs | $T_g$ (°C), 0.5 vol% MWCNTs | $T_g$ (°C), 1.5 vol% MWCNTs |
|---|---|---|---|---|
| $NE_{control}$ | 115.2 | – | – | – |
| $NE_{raw-CNT}$ | – | 114.3 | 113.7 | 113.5 |
| $NE_{O-CNT}$ | – | 119.5 | 122.7 | 119.2 |
| $NE_{PGE-CNT}$ | – | 120.8 | 126.6 | 122.1 |

characteristics also suggested the activation of toughening mechanisms, such as crazing retardation, crack deflection, and pinning of brittle fracture propagation [30]. Nanotube agglomerates, debonding, and telescopic pullout [31,32] were absent from the fracture surfaces of these samples. The MWCNTs appeared as separated bright, high-contrast spots, with an average tube-to-tube distance of ~1–2 μm (Fig. 2c and d).

Incorporation of less than 1.5 vol% of MWCNTs into the epoxy matrix triggered divergent changes in the glass transition temperature ($T_g$) of the NEs. DSC measurements revealed that $T_g$ increased with increasing MWCNT loading for both o-CNT and PGE-CNT reinforced composites, although $T_g$ showed a decrease at 1.5 vol% compared with 0.5 vol% (Table 1). On the other hand, $T_g$ consistently decreased with nanotube concentration in raw-CNT filled NEs.

The trends observed in the measured $T_g$ values were attributed to the altered mobility of the molecular chains or chain sectors in the NEs and were consistent with SEM observations. The increase in glass transition temperature in o-CNT and PGE-CNT composites originated from multiple causes. First, the incorporation of MWCNTs into polymer matrix restricted the mobility of near-interface molecules, as reported for similar systems [33,34]. Secondly, carboxyls and beta-hydroxyls on the functionalized MWCNT surface increased the local cross-linking density [35]. In contrast, the larger free volume resulting from CNT agglomeration and poor interface affinity accounted for the decrease in $T_g$ observed for composites reinforced with raw CNTs. Similarly, the epoxies with 1.5 vol% o-CNTs and PGE-CNTs both exhibited slightly decreased $T_g$ values compared with lower loadings, and this was also attributed to the presence of agglomerations at high CNT loading.

The tensile modulus and fracture strength of the NE specimens are illustrated in Fig. 3 (each point represents the average of five test values). Linear increases in stress–strain curve and composite tensile modulus with respect to nanotube volume fractions were observed for all three systems. Although the composites with raw-CNTs and o-CNTs exhibited similar increases in modulus, the tensile strength of the NEs with raw-CNTs decreased, an indication of CNT agglomerations and poor CNT/epoxy interface stress transfer. The strength data for both o-CNT and PGE-CNT was linear up to 0.5 vol% CNT loadings (Fig. 3), but the data ceased to be linear at 1.5 vol%. Nevertheless, PGE-CNT composites with 1.5 vol% CNTs exhibited modulus and strength increments of ~30% and ~60%, respectively. With judiciously functionalized nano-fillers [35], PGE-CNT reinforced epoxy exhibited the highest reinforcement efficiency of the samples tested.

The predicted composite moduli based on Halpin–Tsai (HT) micromechanics [36,37] were compared with the experimental values of the NEs (Fig. 3a). For these calculations, a modulus of 700 GPa [12] and an aspect ratio of 100 for MWCNTs was assumed [27], and the elastic modulus of the epoxy was taken as 3.1 GPa. The observed modulus values for the NEs ranged between the values predicted by Halpin and Pagano (H–P model for randomly oriented fibers, 1968) and those given by Halpin–Tsai, which constitute a lower bond ($E_{yy}$). Over-estimation of modulus values of nanocomposites is not uncommon among recent reports [38,39], and this variance may be associated with the inherent nanotube waviness and agglomeration of CNTs, which was not included in this model [40,41]. The relevant equations are given below.

Halpin–Tsai model ($E_{xx}$ and $E_{yy}$)

$$E_{xx \text{ or } yy} = (1 + \zeta\eta V_{CNT})E_m/(1 - \eta V_{CNT})$$
$$\eta = (E_{CNT}/E_m - 1)/(E_{CNT}/E_m + \zeta)$$
$$\zeta = 2l/t + 40V_{CNT}^{10} (for E_{xx}) \text{ and } 2w/t + 40V_{CNT}^{10} (\text{for } E_{yy})$$

Halpin–Pagano model (H–P)

$$E_{m'} = 3E_{xx}/8 + 5E_{yy}/8$$

In the equations, $V$ and $E$ refer to the volume percentage and the modulus of the individual phase under discussion. $x$ and $y$ refer to the directions parallel and perpendicular to nanotube orientation, respectively, $l$ is the $CNT$ length, $w$, $t$: width and height of the filler or $CNT$ diameter here, and $CNT$, $m$, and $m$ subscripts' denote the property for nanotubes, epoxy matrix, and the NE, respectively. Because predictions based on the HT model and the HP model fail to provide an accurate estimate for the elastic moduli of NEs, the experimental data were linearly fitted and the following empirical formulae were obtained:

Empirical formula for o-CNT (EO) $E_{m'} = V_m E_m + 1/14.5 V_{CNT} E_{CNT}$
Empirical formula for PGE-CNT (EP) $E_{m'} = V_m E_m + 1/8.5 V_{CNT} E_{CNT}$

### 3.3. Multi-scale reinforced composite laminates (MSRs)

SEM images of MSR fracture surfaces revealed that the inclusion of 0.5vol% MWCNTs in NE enhanced fiber–matrix adhesion and increased surface irregularity (Fig. 4), Incorporation of MWCNTs resulted in fracture surfaces with more "ductile" appearances

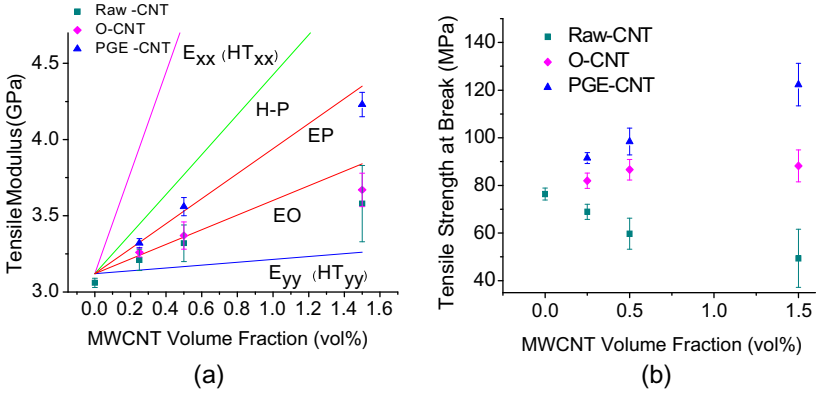


**Fig. 3.** (a) Experimental tensile stress vs. CNT volume fraction plotted with theoretical predictions and (b) experimental tensile strength at break vs. CNT volume fraction.

compared to the clean debonded surface characteristic of the control samples. For samples reinforced with raw-CNTs, debonded regions were observed on basalt fiber surfaces (indicated by arrows in Fig. 4b), indicating the CNT-rich region and CNT-free regions in the raw-CNT filled NE (Fig. 2b). In contrast, the fracture surfaces of MSR samples containing both o-CNT and PGE-CNT reinforced MSRs, revealed basalt fibers that were covered with an interfacial NE layer and a complete absence of debonded regions.

The distribution of o-CNTs and PGE-CNTs on the fracture surfaces revealed that re-distribution and re-orientation of the functionalized CNTs had occurred during MSR laminate processing, which included impregnation, drum-winding, and hot-pressing (Fig. 4e and f). For example, o-CNT nanocomposites exhibited a uniform NE layer with individually dispersed CNTs at the basalt fiber fracture surface (Fig. 4e). Based on the average 2-D inter-tube distance, the local o-CNT loading at the interface was estimated to be as high as 5–6 vol% (as opposed to CNT loading of 0.5 vol%). The observations revealed a preferential distribution of o-CNTs around basalt fibers and the formation of an interphase layer characterized by high CNT loading. The high CNT loading in the interphase layer was induced by the CNT surface modification and the processing conditions. In contrast, few PGE-CNTs were observed on basalt fibers exposed on fracture surfaces (Fig. 4f).

Because of strong interfacial bonding between the PGE-CNT and the epoxy matrix, CNT debonding along the sidewall at the CNT-matrix interface was not observed. The scarcity of the PGE-CNTs observed on basalt fiber surfaces was attributed to the alignment of PGE-CNTs along the fiber direction. Although the exact cause of the alignment is not well understood and awaits further investigation, CNT surface functionalities and shear flow within micron-sized inter-fiber channels during fabrication must play important roles in aligning and dispersing the PGE-CNTs. Additional evidence for the alignment of PGE-CNTs comes from the measured mechanical properties, described next.

Similar to NE samples, the stress–strain curves for MSR specimens are linear, and the results of tensile tests for the multi-scale composites laminates are summarized in Table 2. Also included in the table, for comparison, are values for epoxy reinforced with attapulgite, a rod-like clay nano-particle (ATT-Clay). Increases in the elastic modulus of approximately 10% were observed for laminates with o-CNT or PGE-CNT modified epoxy at 0.225 vol% overall nanotube volume fraction (CNTs account for 0.5 vol% of the NE, and the volume fraction of the NE in the MSR is 45 vol%.). The o-CNT and PGE-CNT reinforced laminates exhibited similar linear increases in elastic modulus with increasing CNT loadings, irrespective of the chemical modification. In contrast, no proportional strength increment was observed at 1.5 vol% CNT loading for both species, a result of the sensitivity of tensile strength to CNT dispersion. In addition, the tensile strength of the o-CNTs reinforced laminates was consistently greater than those with PGE-CNTs. This

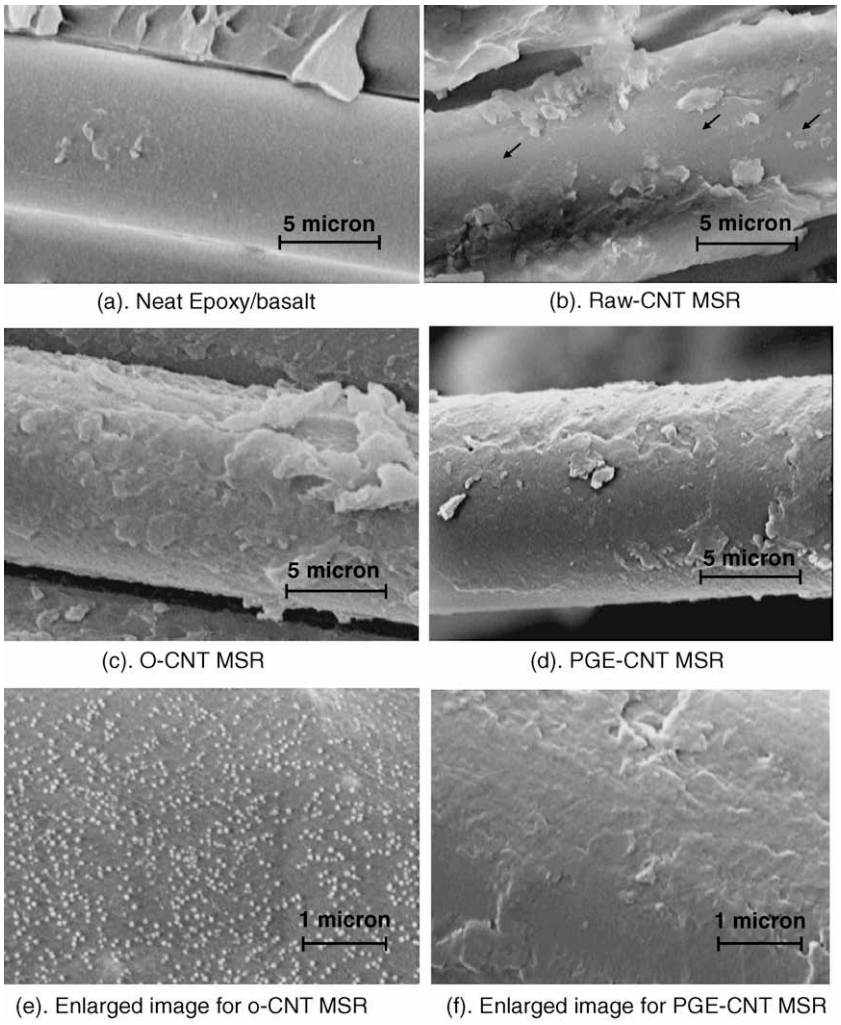


**Fig. 4.** SEM images of basalt fiber fracture surface of MSRs with 0.5 vol% CNT inclusions.

**Table 2**
Young's modulus and tensile strength values for MSR specimens.

| Epoxy/basalt laminates | Young's modulus (GPa) | % improvement | Tensile strength (MPa) | % improvement |
|---|---|---|---|---|
| Control laminate 0 vol% | 27.65 ± 0.41 | 0 | 584.7 ± 10.3 | 0 |
| raw CNT 0.5 vol% | 27.44 ± 0.76 | −0.76 | 564.0 ± 31.0 | −3.54 |
| o-CNT 0.5 vol% | 30.41 ± 1.31 | +9.98 | 635.7 ± 33.8 | +8.72 |
| PGE-CNT 0.5 vol% | 29.92 ± 0.83 | +8.20 | 608.8 ± 20.0 | +3.98 |
| raw-CNT 1.5 vol% | 28.53 ± 1.18 | +3.73 | 504.0 ± 42.0 | −13.8 |
| o-CNT 1.5 vol% | 36.4 ± 0.97 | +31.65 | 627.7 ± 25.5 | +7.35 |
| PGE-CNT 1.5 vol% | 34.90 ± 0.77 | +26.2 | 615.1 ± 19.7 | +5.20 |
| ATT-clay 1.25 vol% | 29.85 ± 1.03 | +7.96 | 530.9 ± 43.4 | −9.20 |
| ATT-clay 2.5 vol% | 28.06 ± 2.62 | +1.48 | 465.4 ± 94.5 | −20.4 |

finding was attributed to superior fiber–matrix stress transfer in the o-CNT MSR samples that resulted from the high CNT loading at the fiber interfaces.

In order to predict the elastic moduli of the MSRs and analyze the experimental values reported above, a conventional micromechanics approach was employed. In this approach, the elastic moduli for the NE matrices were adopted based on the effective properties from the EO, EP, and HP predictions. Subsequently, the Rule of Mixtures (ROM) and Inverse Rule of Mixtures (IROM) was used to determine the elastic moduli of a single ply at different CNT loadings (vol% of CNT in NEs).

$$E'_{11} = V_f E_f + V_{m'} E_{m'} \quad \text{(ROM)}$$
$$E'_{22} = (V_f E_f + V_{m'} E_{m'})^{-1} \quad \text{(IROM)}$$

In the expression, 1 and 2 refer to the fiber direction and the direction perpendicular to fiber orientation, respectively. The basalt fiber loading for all samples was calculated to be ~55 vol%, and the elastic modulus for basalt fiber was taken as 85 GPa. The prime symbol and the subscripts $f$ denote the property of a single ply and fiber, respectively.

The elastic properties of the multi-scale composite laminates (denoted $E_c$, the subscript $c$ refers to the composite laminate) are calculated using a micromechanics formulation and assuming plane strain. A composite reinforced with continuous unidirectional fibers in which all fibers are aligned along the one direction is treated as a transversely isotropic material with three planes of symmetry.

For layers with fiber direction parallel to one (layer No. 1, 4 in a 0/90/90/0 composite laminate):

$$\begin{Bmatrix} \sigma_1 \\ \sigma_2 \\ \sigma_3 \\ \tau_{23} \\ \tau_{13} \\ \tau_{12} \end{Bmatrix} = \begin{bmatrix} Q_{11} & Q_{12} & Q_{12} & 0 & 0 & 0 \\ Q_{12} & Q_{22} & Q_{23} & 0 & 0 & 0 \\ Q_{12} & Q_{23} & Q_{22} & 0 & 0 & 0 \\ 0 & 0 & 0 & \frac{Q_{22}-Q_{23}}{2} & 0 & 0 \\ 0 & 0 & 0 & 0 & Q_{66} & 0 \\ 0 & 0 & 0 & 0 & 0 & Q_{66} \end{bmatrix} \begin{Bmatrix} \varepsilon_1 \\ \varepsilon_2 \\ \varepsilon_3 \\ \gamma_{23} \\ \gamma_{13} \\ \gamma_{12} \end{Bmatrix}$$

At plane strain conditions:

$$\sigma_3 = 0$$
$$\tau_{23} = 0$$
$$\tau_{12} = 0$$

We have:

$$\begin{Bmatrix} \sigma_1 \\ \sigma_2 \\ \tau_{12} \end{Bmatrix} = \begin{bmatrix} Q_{11} & Q_{12} & 0 \\ Q_{12} & Q_{22} & 0 \\ 0 & 0 & Q_{66} \end{bmatrix} \begin{Bmatrix} \varepsilon_1 \\ \varepsilon_2 \\ \gamma_{12} \end{Bmatrix}$$

Filling in the elastic constants for transversely isotropic materials:

$$\begin{Bmatrix} \sigma_1 \\ \sigma_2 \\ \tau_{12} \end{Bmatrix} = \begin{bmatrix} \frac{E'_{11}}{D} & \frac{\upsilon_{12}E'_{22}}{D} & 0 \\ \frac{\upsilon_{12}E'_{22}}{D} & \frac{E'_{22}}{D} & 0 \\ 0 & 0 & G_{12} \end{bmatrix} \begin{Bmatrix} \varepsilon_1 \\ \varepsilon_2 \\ \gamma_{12} \end{Bmatrix}$$

Similarly, for layers with fiber direction perpendicular to 1 (or layer No. 2, 3):

$$\begin{Bmatrix} \sigma_1 \\ \sigma_2 \\ \tau_{12} \end{Bmatrix} = \begin{bmatrix} \frac{E'_{22}}{D} & \frac{\upsilon_{12}E'_{22}}{D} & 0 \\ \frac{\upsilon_{12}E'_{22}}{D} & \frac{E'_{11}}{D} & 0 \\ 0 & 0 & G_{12} \end{bmatrix} \begin{Bmatrix} \varepsilon_1 \\ \varepsilon_2 \\ \gamma_{12} \end{Bmatrix}$$

$D = 1 - \upsilon_{12}\upsilon_{21} = \sim 0.945$ ($\upsilon_{12}$, $\upsilon_{21}$ were estimated based on Refs. [42,43]).

Because of the symmetry of the MSR composite laminae (symmetric balanced cross-ply), the calculation of the laminate elastic moduli for the longitudinal direction (direction 1) is reduced to the following relationship when the strain in the direction 2 is small. A similar result can be deduced for the transverse direction:

$$E_{c11} = E_{c22} = (E'_{11} + E'_{22})/2D$$

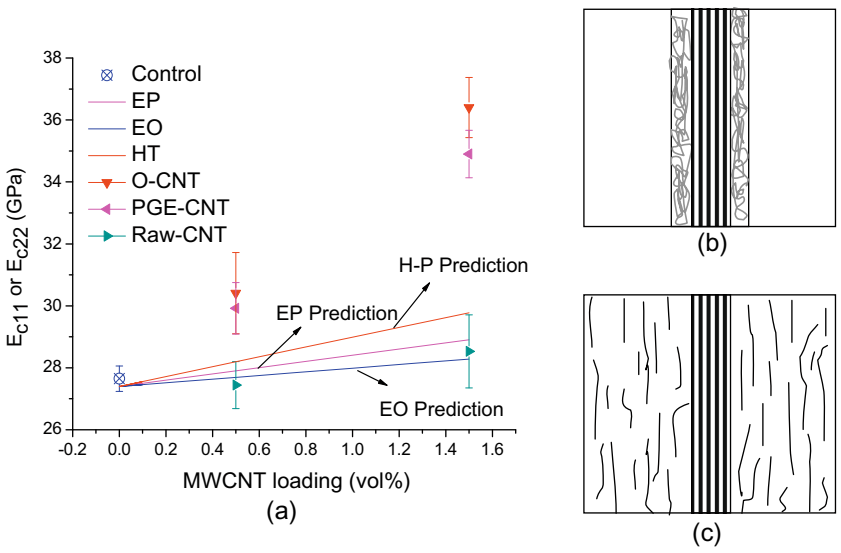


**Fig. 5.** (a) $E_{c11}$ vs. CNT volume loading: measured values and predicted curves, (b) CNT redistribution around basalt fiber and (c) CNT alignment along basalt fiber orientation.

The $E_c$ vs. CNT loading relationship is illustrated by the measured values plotted in Fig. 5a. The curves plotted are the predictions from the micromechanics model, which significantly underestimates the elastic properties for fiber-dominated directions (both $E_{c11}$ and $E_{c22}$ for cross-ply laminates). Conventional wisdom dictates that MWCNT reinforcements should be most effective in boosting matrix-dominated properties, such as interlaminar shear modulus, $G_{IC}$, and $G_{IIC,}$ particularly when used as nano-scale additives in fiber-reinforced composites [44,45]. However, current predictions underestimate the ~20% per vol% (vol% of CNT in NE) increase observed in the elastic modulus of the composite laminates. Therefore, additional reinforcing mechanisms must be considered.

The o-CNT re-distribution and the apparent PGE-CNT alignment observed in Fig. 4 and portrayed in Fig. 5b and c provide insight into the underlying causes of the discrepancies between the measured modulus values and predictions from the micromechanics model. The annular interphase regions around basalt fibers (with high o-CNT loadings) provides a high modulus layer around basalt fibers, the elastic modulus of which can be as high as 10–20 GPa (H–P, $E_{xx}$) based on the estimation of 5 vol% CNT concentration on basalt fiber surface. A higher interfacial shear modulus (~1/3 of the tensile modulus of the NE) also improves the interfacial stress transfer properties between the NE and basalt fibers and, consequently, enhances the elastic modulus and strength. On the other hand, micromechanical predictions are consistent with the alignment of PGE-CNTs along the direction of basalt fibers as indicated by the SEM observations (Fig. 4). An effective matrix elastic modulus of ~4.7 GPa can be deduced based on 0.5 vol% of aligned and straight CNTs ($E_{xx}$). Using the same micromechanics model employed above, the estimated $E_{c11}$ (at 0.5 vol%) of ~29.3 GPa is within the experimentally measured range of longitudinal elastic modulus values for PGE-CNT reinforced MSR (Fig. 5a). Thus, the unusually high reinforcement efficiency of the functionalized MWCNTs for fiber-dominated properties of multi-scale reinforced composite laminates is attributed to the re-distribution or re-orientation of CNTs under processing conditions.

## 4. Conclusions

Appropriate choice of surface groups led to uniform dispersion and covalent integration of MWCNTs into a DGEBA epoxy system. Tensile tests of the bulk NEs revealed increases in both elastic modulus and strength, albeit lower than theoretical predictions due to natural CNT waviness and partial agglomeration.

Direct incorporation of functionalized MWCNTs into epoxy/basalt composite laminates improved the elastic properties of the composites, particularly in the fiber direction, and this increase was not predicted by a classical micromechanics analysis based on the equivalent matrix properties obtained from NE specimens. SEM observations revealed an unexpected re-distribution and re-orientation of CNTs resulting from processing. When properly positioned and oriented within the matrix, carbon nanotube reinforcement markedly influenced properties that are usually dominated by fiber reinforcements. In-situ alignment of carbon nanotubes and formation of a distinct, hardened, annular interphase around basalt fibers were instrumental in attaining the high reinforcement efficiency in the fiber-dominated direction of these hierarchical composites.

## Acknowledgements

This work was supported by the Merwyn C. Gill Foundation. We are grateful to Professor K.S. Shing and Tao Wei for their assistance in preparing transmission samples for FTIR. We are also grateful to Alicia Thompson and John Curulli for their kind assistance with TEM and SEM characterization.

## References

[1] Sgriccia N, Hawley MC. Thermal, morphological, and electrical characterization of microwave processed natural fiber composites. Compos Sci Technol 2007;67(9):1986–91.
[2] Silva C, Marotta E, Schuller M, Peel L, O'Neill M. In-plane thermal conductivity in thin carbon fiber composites. J Thermophys Heat Transf 2007;21(3):460–7.
[3] Ogihara S, Uehara T. Mechanical properties of SMA fiber/epoxy composite. J Mater Sci Lett 2003;22(9):683–5.
[4] Park JS, Park SS, Lee S. Thermal and mechanical properties of carbon fiber reinforced epoxy composites modified with CTBN and hydroxyl terminated polyester. Adv Polym Emerg Technol 2007:568–72.
[5] Huang L, Wang C, Lu YF. Thermal and moisture adsorption properties of cyanate ester modified epoxy resin and fiber–glass composites. J Reinf Plast Compos 2008;27(7):725–38.
[6] Dilandro L, Dibenedetto AT, Groeger J. The effect of fiber–matrix stress transfer on the strength of fiber-reinforced composite materials. Polym Compos 1988;9(3):209–21.
[7] Boogh LCN, Meier RJ, Kausch HH, Kip BJ. A Raman microscopy study of stress transfer in high-performance epoxy composites reinforced with polyethylene fibers. J Polym Sci B 1992;30(4):325–33.
[8] Mathur RB, Chatterjee S, Singh BP. Growth of carbon nanotubes on carbon fibre substrates to produce hybrid/phenolic composites with improved mechanical properties. Compos Sci Technol 2008;68(7–8):1608–15.
[9] Bekyarova E, Thostenson ET, Yu AP, Itkis ME, Fakhrutdinov D, Chou TW, et al. Functionalized single-walled carbon nanotubes for carbon fiber–epoxy composites. J Phys Chem C 2007;111(48):17865–71.
[10] Dean D, Obore AM, Richmond S, Nyairo E. Multiscale fiber-reinforced nanocomposites: synthesis, processing and properties. Compos Sci Technol 2006;66(13):2135–42.
[11] Kim YA, Kamio S, Tajiri T, Hayashi T, Song SM, Endo M, et al. Enhanced thermal conductivity of carbon fiber/phenolic resin composites by the introduction of carbon nanotubes. Appl Phys Lett 2007;90(9):93125-1–-3.
[12] Yu MF, Lourie O, Dyer MJ, Moloni K, Kelly TF, Ruoff RS. Strength and breaking mechanism of multiwalled carbon nanotubes under tensile load. Science 2000;287(5453):637–40.
[13] Bekyarova E, Thostenson ET, Yu A, Kim H, Gao J, Tang J, et al. Multiscale carbon nanotube–carbon fiber reinforcement for advanced epoxy composites. Langmuir 2007;23(7):3970–4.
[14] Thostenson ET, Li WZ, Wang DZ, Ren ZF, Chou TW. Carbon nanotube/carbon fiber hybrid multiscale composites. J Appl Phys 2002;91(9):6034–7.
[15] Qiu JJ, Zhang C, Wang B, Liang R. Carbon nanotube integrated multifunctional multiscale composites. Nanotechnology 2007;18(27):275708.
[16] Gojny FH, Wichmann MHG, Fiedler B, Bauhofer W, Schulte K. Influence of nano-modification on the mechanical and electrical properties of conventional fibre-reinforced composites. Composites: Part A 2005;36(11):1525–35.
[17] Veedu VP, Cao AY, Li XS, Ma KG, Soldano C, Kar S, et al. Multifunctional composites using reinforced laminae with carbon-nanotube forests. Nat Mater 2006;5(6):457–62.
[18] Garcia EJ, Wardle BL, Hart AJ. Joining prepreg composite interfaces with aligned carbon nanotubes. Compos: Part A 2008;39:1065–70.
[19] Thostenson ET, Ren ZF, Chou TW. Advances in the science and technology of carbon nanotubes and their composites: a review. Compos Sci Technol 2001;61(13):1899–912.
[20] Jonathan N, Coleman UK, Yurii K, Gun K. Mechanical reinforcement of polymers using carbon nanotubes. Adv Mater 2006;18:689–706.
[21] Paiva MC, Zhou B, Fernando KAS, Lin Y, Lopes PE, Pennington WT, et al. Physical and mechanical characterization of nanocomposites with carbon nanotubes functionalized with the matrix polymer. Compos Interf 2005;12(8–9):757–68.
[22] Frankland SJV, Caglar A, Brenner DW, Griebel M. Molecular simulation of the influence of chemical cross-links on the shear strength of carbon nanotube–polymer interfaces. J Phys Chem B 2002;106:3046–8.
[23] Miaudet P, Badaire S, Maugey M, Derre A, Pichot V, Launois P, et al. Hot-drawing of single and multiwall carbon nanotube fibers for high toughness and alignment. Nano Lett 2005;5(11):2212–5.
[24] Camponeschi E, Vance R, Al-Haik M, Garmestani H, Tannenbaum R. Properties of carbon nanotube–polymer composites aligned in a magnetic field. Carbon 2007;45(10):2037–46.
[25] Hilding JM, Hong MPL, Grullke EA. Alignment of dispersed multiwalled carbon nanotubes in low strength AC electrical fields. J Nanosci Nanotechnol 2005;5(5):742–6.
[26] Chen W, Auad ML, Williams RJJ, Nutt SR. Improving the dispersion and flexural strength of multiwalled carbon nanotubes–stiff epoxy composites through β-hydroxyester surface functionalization coupled with the anionic homopolymerization of the epoxy matrix. Euro Polym J 2006;42:2765–72.
[27] Liu J, Rinzler AG, Dai H, Hafner JH, Bradley RK, Boul PJ, et al. Fullerene pipes. Science 1998;280:1253–6.
[28] Fisher FT, Eitan A, Andrews R, Brinson LC, Schadler LS. Reinforcement mechanisms in MWCNT-filled polycarbonate. Compos Sci Technol 2006;66(9):1159–70.

[29] Ellis B. Chemistry and technology of epoxy resins. Glasgow (UK): Blackie Academic & Professional; 1993 [Chapter 3].
[30] Kuzumaki T, Mitsuda Y. Measurement of electrical conductivity upon in situ telescopic deformation of multiwall carbon nanotube. Carbon 2005;43(10):2227–9.
[31] Cumings J, Zettl A. Localization and nonlinear resistance in telescopically extended nanotubes. Phys Rev Lett 2004;93(8):086801-1–1-4.
[32] Xia Z, Riester L, Curtin WA, Li H, Sheldon BW, Liang J, et al. Direct observation of toughening mechanisms in carbon nanotube ceramic matrix composites. Acta Mater 2004;52(4):931–44.
[33] Gojny FH, Schulte K. Functionalisation effect on the thermo-mechanical behaviour of multi-wall carbon nanotube/epoxy-composites. Compos Sci Technol 2004;64(15):2303–8.
[34] Wang JG, Fang ZP, Gu AJ, Xu LH, Li F. Effect of amino-functionalization of multi-walled carbon nanotubes on the dispersion with epoxy resin matrix. J Appl Polym Sci 2006;100(1):97–104.
[35] Chen W, Lu HB, Nutt SR. The Influence of functionalized MWCNT reinforcement on the thermomechanical properties and morphology of epoxy nanocomposites. Compos Sci Technol; in press. doi: 10.1016/j.compscitech.2008.05.011.
[36] Gojny FH, Wichmann MHG, Kopke U, Fiedler B, Schulte K. Carbon nanotube-reinforced epoxy-composites: enhanced stiffness and fracture toughness at low nanotube content. Compos Sci Technol 2004;64(15):2363–71.
[37] Li XD, Gao HS, Scrivens WA, Fei DL, Xu XY, Sutton MA, et al. Reinforcing mechanisms of single-walled carbon nanotube-reinforced polymer composites. J Nanosci Nanotechnol 2007;7(7):2309–17.
[38] Garcia EJ, Hart AJ, Wardle BL, Slocum AH. Fabrication and nanocompression testing of aligned carbon-nanotube-polymer nanocomposites. Adv Mater 2007;9(16):2151–6.
[39] Thostenson ET, Chou TW. On the elastic properties of carbon nanotube-based composites: modelling and characterization. J Phys: D 2003;6(5):573–82.
[40] Fisher FT, Bradshaw RD, Brinson LC. Effects of nanotube waviness on the modulus of nanotube-reinforced polymers. Appl Phys Lett 2002;80(24):4647–9.
[41] Anumandla V, Gibson RFA. Comprehensive closed form micromechanics model for estimating the elastic modulus of nanotube-reinforced composites. Compos Part A: Appl Sci Manuf 2006;37:2178–85.
[42] Shan HZ, Chou TW. Transverse elastic moduli of unidirectional fiber composites with fiber/matrix interfacial debonding. Compos Sci Technol 1995;53(4):383–91.
[43] Mead DJ, Joannides RJ. Measurement of the dynamic moduli and Poisson's ratios of a transversely isotropic fibre-reinforced plastic. Composites 1991;22(1):15–29.
[44] Khabashesku VN, Barrera EV, Zhu J, Imam A, Crane R, Lozano K. Processing a glass fiber reinforced vinyl ester composite with nanotube enhancement of interlaminar shear strength. Compos Sci Technol 2007;67(7–8):1509–17.
[45] Wichmann MHG, Sumfleth J, Gojny FH, Quaresimin M, Fiedler B, Schulte K. Glass–fibre-reinforced composites with enhanced mechanical and electrical properties – benefits and limitations of a nanoparticle modified matrix. Eng Fract Mech 2006;73(16):2346–59.